



*Supplement of*

## **The Global Methane Budget 2000–2017**

**Marielle Saunois et al.**

*Correspondence to:* Marielle Saunois ([marielle.saunois@lsce.ipsl.fr](mailto:marielle.saunois@lsce.ipsl.fr))

The copyright of individual parts of the supplement might differ from the CC BY 4.0 License.

<b>1</b>	<b>Supplementary Text 1: Atmospheric observations .....</b>	<b>2</b>
<b>2</b>	<b>Supplementary Text 2: Principle of inversions .....</b>	<b>5</b>
<b>3</b>	<b>Supplementary Text 3: Set of prior fluxes suggested by the atmospheric inversion protocol .....</b>	<b>6</b>
<b>4</b>	<b>Supplementary Text 4: Wetland emissions from land surface models and wetland extent .....</b>	<b>7</b>

### **List of Tables**

Table S1	List of the countries used to define the 18 continental regions .....	9
Table S2	Assignment of the inventory specific sectors to GCP sub- and main categories .....	10
Table S3	Contributions of the biogeochemical models to the different releases of the global methane budget.....	12
Table S4	CCMI models used to estimate OH tropospheric mass-weighted concentrations, methane losses and lifetime. Average over 2000-2010 (Zhao et al., 2019).....	13
Table S5	Soil uptake estimates from the literature and in this GCP synthesis in Tg CH <sub>4</sub> yr <sup>-1</sup> .....	15
Table S6	Set-up of the different inverse systems contributing to this study. ....	16
Table S7	Contributions of the different inverse systems to the different releases of the global methane budget.....	24

### **List of figures**

Figure S1	Map of the 18 continental regions. 1: USA; 2: Canada; 3: Central America; 4: Northern South America; 5: Brazil; 6:Southwest Southern America; 7: Europe; 8: Northern Africa; 9: Equatorial Africa; 10: Southern Africa; 11: Russia; 12: Central Asia; 13: Middle East; 14: China; 15: Korea and Japan; 16: South Asia; 17: South East Asia; 18: Oceania.....	25
-----------	--	----

Figure S2 Comparison of the distribution of methane emissions from termite en mg CH<sub>4</sub> m<sup>-2</sup> day<sup>-1</sup>.  
Emission distribution from Sanderson et al. (1999), Saunois et al. (2016) and this study. The  
numbers represent the total annual termite emissions for each distribution. ..... 26

## 1 Supplementary Text 1: Atmospheric observations

### Existing satellite data other than GOSAT, already presented in the main text

#### Column average XCH<sub>4</sub> - SCIAMACHY

Between 2003 and 2012, the Scanning Imaging Absorption spectrometer for Atmospheric CartographHY (SCIAMACHY) was operated on board the ESA ENVIRONMENTAL SATellite (ENVISAT), providing nearly 10 years of XCH<sub>4</sub> sensitive to the atmospheric boundary layer (Burrows et al., 1995; Buchwitz et al., 2006; Dils et al., 2006; Frankenberg et al., 2011). These satellite retrievals were the first to be used for global and regional inverse modelling of methane fluxes (Meirink et al., 2008a; Bergamaschi et al., 2007; Bergamaschi et al., 2009). The relatively long-term record allowed the analysis of the inter-annual methane variability (Bergamaschi et al., 2013). However, the use of SCIAMACHY necessitates important bias correction, especially after 2005 (up to 40 ppb from south to north) (Bergamaschi et al., 2013; Houweling et al., 2014; Alexe et al., 2015).

#### Mid-to-upper troposphere CH<sub>4</sub> columns - IASI

In 2006, 2012 and 2018, the Infrared Atmospheric Sounding Interferometer (IASI) on board the European MetOp,A, B and C satellites have started to operate. Measuring the thermal radiation from Earth and the atmosphere in the TIR, they provide mid-to-upper troposphere columns of methane (representative of the 5-15 km layer) over the tropics using an infrared sounding interferometer (Crevoisier et al., 2009). Despite their sensitivity being limited to the mid-to-upper troposphere, their use in flux inversions has shown consistent results in the tropics with surface and other satellite-based inversions (Cressot et al., 2014).

#### Other surface based atmospheric observations

Other types of methane measurements are available. These are not commonly used to infer fluxes from global inversions (yet), but are used to verify their performance (see e.g. Bergamaschi et al. (2013)). Aircraft or balloon-borne in situ measurements can deliver vertical profiles with high vertical resolution. Some studies made use of aircraft profiles to estimate local to regional methane

emissions (e.g. Karion et al., 2015; Peischl et al., 2016; Wilson et al., 2016; Gvakharia et al., 2017). Such observations can also be used to evaluate remote sensing measurements from space or from the surface and bring them on the same scale as the in situ surface measurements (e.g., Wunch et al., 2010). Aircraft measurements have been undertaken in various regions either during campaigns (Wofsy, 2011; Beck et al., 2012; Chang et al., 2014; Paris et al., 2010), or in a recurrent mode using small aircrafts (Sweeney et al., 2015; Umezawa et al., 2014; Gatti et al., 2014) and commercial aircrafts (Schuck et al., 2012; Brenninkmeijer et al., 2007; Umezawa et al., 2012; 2014; Machida et al., 2008). Balloons can carry in situ instruments (e.g. Joly et al. (2008); using tunable laser diodes spectrometry) or air samplers such as AirCores that are rapidly developing in North America and Europe (Karion et al., 2010; Membrive et al., 2017; Andersen et al., 2018), allowing the measurement of vertical profiles up to 30 km height. New technologies have also developed systems based on cavity ring down spectroscopy (CRDS), opening a large ensemble of new activities to estimate methane emissions such as drone measurements (using a lightweight version of CRDS), as land-based vehicles for real-time, mobile monitoring over oil and gas facilities, as well as ponds, landfills, livestock, (e.g. Ars et al., 2017).

The Total Carbon Column Observing Network (TCCON) uses ground-based Fourier transform spectrometers (FTS) to measure atmospheric column abundances of CO<sub>2</sub>, CO, CH<sub>4</sub>, N<sub>2</sub>O and other molecules that absorb sunlight in the near-infrared spectral region (e.g. Wunch et al., 2011). As TCCON measurements make use of sunlight, they can be performed throughout the day during clear sky conditions, with the sun typically 10° above the horizon. The TCCON network has been established as a reference for the validation of column retrievals, like those from SCIAMACHY, GOSAT, and TROPOMI (e.g., Butz et al., 2011, Morino et al., 2011). TCCON data can be obtained from the TCCON Data Archive, hosted by CaltechDATA (<https://tccondat.org/>).

### Methane isotope observations

The processes emitting methane discriminate between its isotopologues (isotopes). The two main stable isotopes of CH<sub>4</sub> are <sup>13</sup>CH<sub>4</sub> and CH<sub>3</sub>D, and there is also the radioactive carbon isotope <sup>14</sup>C-CH<sub>4</sub>. Isotopic signatures are conventionally given by the deviation of the sample mole ratio (for example, R=<sup>13</sup>CH<sub>4</sub>/<sup>12</sup>CH<sub>4</sub> or CH<sub>3</sub>D/CH<sub>4</sub>) relative to a given standard (R<sub>std</sub>) relative to a reference ratio, given in per mil as in Eq. 1.

$$\delta^{13}\text{CH}_4 \text{ or } \delta D(\text{CH}_4) = \left( \frac{R}{R_{\text{std}}} - 1 \right) \times 1000 \quad (1)$$

For the <sup>13</sup>CH<sub>4</sub> isotope, the conventional reference standard is known as Vienna Pee Dee Belemnite (VPDB), with R<sub>std</sub>=0.0112372. The same definition applies to CH<sub>3</sub>D, with the Vienna Standard

Mean Ocean Water (VSMOW)  $R_{\text{SMOW}}=0.00015575$ . The isotopic composition of atmospheric methane is measured at a subset of surface stations (Quay et al., 1991; 1999; Lowe et al., 1994; Miller et al., 2002; Morimoto et al., 2006; Tyler et al., 2007). The mean atmospheric values are about -47‰ for  $\delta^{13}\text{CH}_4$  and -86 to -96‰ for  $\delta\text{D}(\text{CH}_4)$ .  $\delta^{13}\text{CH}_4$  measurements are made mainly on flask air samples analysed with gas-chromatograph isotope ratio spectrometry for which an accuracy of 0.05 per mil for  $\delta^{13}\text{CH}_4$  and 1.5‰ for  $\delta\text{D}(\text{CH}_4)$  can be achieved (Rice et al., 2001; Miller et al., 2002). These isotopic measurements based on air flask sampling have relatively low spatial and temporal resolutions. Laser-based absorption spectrometers and isotope ratio mass spectrometry techniques have recently been developed to increase sampling frequency and allow in situ operation (McManus et al., 2010; Santoni et al., 2012), and first continuous time series of  $\delta^{13}\text{CH}_4$  have been reported in Europe (Röckmann et al., 2016).

Measurements of  $\delta^{13}\text{CH}_4$  can help to partition the different methanogenic processes of methane: biogenic (-70‰ to -55‰), thermogenic (typically -55‰ to -25‰, but down to -70‰ considering early thermogenic gas; Milkov and Etiope, 2018) or pyrogenic (-25‰ to -15‰) sources (Quay et al., 1991; Miller et al., 2002; Fisher et al., 2011) or even the methanogenic pathway (McCalley et al., 2014).  $\delta\text{D}(\text{CH}_4)$  provides valuable information on the oxidation by the OH radicals (Röckmann et al., 2011) due to a fractionation of about 300‰. Emissions also show substantial differences in  $\delta\text{D}(\text{CH}_4)$  isotopic signatures: -200‰ for biomass burning sources versus -360 to -250‰ for biogenic sources (Melton et al., 2012; Quay et al., 1999).  $^{14}\text{C}-\text{CH}_4$  measurements (Quay et al., 1991; 1999; Lowe et al., 1988) may also help to partition for fossil fuel contribution (radiocarbon free source). For example, Lassey et al. (2007a) used more than 200 measurements of radioactive  $^{14}\text{C}-\text{CH}_4$  (with a balanced weight between Northern and Southern hemispheres) to further constrain the fossil fuel contribution to the global methane source emission to 30±2% for the period 1986-2000.

Integrating isotopic information is important to improve our understanding of the methane budget. Some studies have simulated such isotopic observations (Neef et al., 2010; Monteil et al., 2011) or used them as additional constraints to inverse systems (Mikaloff Fletcher et al., 2004; Hein et al., 1997; Bergamaschi et al., 2000; Bousquet et al., 2006; Neef et al., 2010; Thompson et al., 2015; McNorton et al., 2018). Using pseudo-observations, Rigby et al. (2012) found that Quantum Cascade Laser-based isotopic observations would reduce the uncertainty in four major source categories by about 10% at the global scale (microbial, biomass burning, landfill and fossil fuel) and by up to 50% at the local scale. Although not all source types can be separated using  $^{13}\text{C}$ ,  $\text{D}$  and  $^{14}\text{C}$  isotopes, such data bring valuable information to constrain groups of sources in atmospheric inversions, if the isotopic signatures of the various sources can be precisely assessed (Bousquet et

al., 2006, supplementary material). More recently, several studies have implemented joint  $^{13}\text{C}$  and  $^{12}\text{C}$  analyses in box models to retrieve trends in methane emissions and sinks (Schaefer et al., 2016; Rice et al., 2016; Schwietzke et al., 2016; Rigby et al., 2017; Turner et al., 2017) and Thompson et al. (2018) proposed a box model analysis including  $\text{CH}_4$ ,  $\text{C}_2\text{H}_6$ , and  $\delta^{13}\text{C}_{\text{CH}4}$ .

## 2 Supplementary Text 2: Principle of inversions

An atmospheric inversion for methane fluxes (sources and sinks) optimally combines atmospheric observations of methane and associated uncertainties, a prior knowledge of the fluxes including their uncertainties, and a chemistry-transport model to relate fluxes to concentrations (Rodgers, 2000). In this sense, top-down inversions integrate all the components of the methane cycle described previously in this paper. The observations can be surface or upper-air in situ observations, satellite and surface retrievals. Prior emissions generally come from bottom-up approaches such as process-based models or data-driven extrapolations (natural sources) and inventories (anthropogenic sources). The chemistry-transport model can be Eulerian or Lagrangian, and global or regional, depending on the scale of the flux to be optimized. Atmospheric inversions generally rely on the Bayes theorem, which leads to the minimization of a cost function as Eq. (2):

$$J(x) = \frac{1}{2} (y - H(x))^T R^{-1} (y - H(x)) + \frac{1}{2} (x - x_b)^T B^{-1} (x - x_b) \quad (2)$$

where  $\mathbf{y}$  is a vector containing the atmospheric observations,  $\mathbf{x}$  is a state vector containing the methane emissions and other appropriate variables (like OH concentrations or  $\text{CH}_4$  concentrations at the start of the assimilation window) to be estimated,  $\mathbf{x}_b$  is the prior state of  $\mathbf{x}$ , and  $H$  is the observation operator, here the combination of an atmospheric transport and chemistry model and an interpolation procedure sampling the model at the measurement coordinates.  $\mathbf{R}$  is the error covariance matrix of the observations and  $\mathbf{P}_b$  is the error covariance matrix associated to  $\mathbf{x}_b$ . The errors on the modelling of atmospheric transport and chemistry are included in the  $\mathbf{R}$  matrix (Tarantola, 1987). The minimization of a linearized version of  $J$  leads to the optimized state vector  $\mathbf{x}_a$  (Eq. 3):

$$x_a = x_b + (H^T R^{-1} H + P_b^{-1})^{-1} H^T R^{-1} (y - H(x)) \quad (3)$$

where  $\mathbf{P}_a$  is given by Eq. 4 and represents the error covariance matrix associated to  $\mathbf{x}_a$ , and  $\mathbf{H}$  contains the sensitivities of any observation to any component of state vector  $\mathbf{x}$  (linearized version of the observation operator  $H(x)$ ).

$$P_a = (H^T R^{-1} H + P_b^{-1})^{-1} \quad (4)$$

Unfortunately, the size of the inverse problem usually does not allow computing  $\mathbf{P}_a$ , which is therefore approximated using the leading eigenvectors of the Hessian of  $J$  (Chevallier et al., 2005) or from stochastic ensembles (Chevallier et al., 2007). Therefore, the optimized fluxes  $\mathbf{x}_a$  are obtained using classical minimization algorithms (Chevallier et al., 2005; Meirink et al., 2008b). Alternatively, Chen and Prinn (2006) computed monthly emissions by applying a recursive Kalman filter in which  $\mathbf{P}_a$  is computed explicitly for each month. Emissions are generally derived at weekly to monthly time scales, and for spatial resolutions ranging from model grid resolution to large aggregated regions. Spatio-temporal aggregation of state vector elements reduces the size of the inverse problem and allows the computation of  $\mathbf{P}_a$ . However, such aggregation can also generate aggregation errors inducing possible biases in the inferred emissions and sinks (Kaminski et al., 2001). The estimated  $\mathbf{x}_a$  can represent either the net methane flux in a given region or contributions from specific source categories. Atmospheric inversions use bottom-up models and inventories as prior estimates of the emissions and sinks in their setup, which make B-U and T-D approaches generally not independent.

### **3 Supplementary Text 3: Set of prior fluxes suggested by the atmospheric inversion protocol**

A set of fluxes for the different methane sources has been gathered and made available to the community to perform atmospheric inversions.

The anthropogenic emissions are from EDGARv4.3.2 database (Janssens-Maenhout et al., 2019), which is available up to 2012. For this study, the EDGARv4.3.2 was extrapolated up to 2017 using the extended FAO-CH<sub>4</sub> emissions for CH<sub>4</sub> emissions from enteric fermentation, manure management and rice cultivation, and using the BP statistical review of fossil fuel production and consumption (<http://www.bp.com/>) to update CH<sub>4</sub> emissions from coal, oil and gas sectors. In this extrapolated inventory, called EDGARv4.3.2<sub>EXT</sub>, methane emissions for year  $t$  are set up equal to the 2012 EDGAR CH<sub>4</sub> emissions ( $E_{EDGARv4.3.2}$ ) times the ratio between the FAO-CH<sub>4</sub> emissions (or BP statistics) of year  $t$  ( $E_{FAO-CH4}(t)$ ) and FAO-CH<sub>4</sub> emissions (or BP statistics) of 2012 ( $E_{FAO-CH4}(2012)$ ). For each emission sector, the region-specific emissions ( $E_{EDGARv4.3.2ext}$ ) in year ( $t$ ) are estimated following Eq. (1):

$$E_{EDGARv4.3.2}(t) = E_{EDGARv4.3.2}(2012) \times E_{FAO-CH4}(t)/E_{FAO-CH4}(2012) \quad (1)$$

Transport, industrial, waste and biofuel sources were linearly extrapolated based on the last three years of data while other sources are kept constant at the 2012 level. This extrapolation approach is

necessary, and often performed by top-down approaches to define prior emissions, because, up to now, global inventories such as sector-specific emissions in the EDGAR database are not updated on a regular basis.

Biomass burning from GFED4.1s was provided on a monthly basis up to 2017.

For wetland emissions, the mean of 11 models of Poulter et al., (2017) from the GCP-CH<sub>4</sub> BU group was calculated and provided as monthly global CH<sub>4</sub> emissions.

Emissions for termites are from the model described in Kirschke et al. (2013), and represent a climatological estimate.

Emissions from oceans are from Lambert and Schmidt (1993), emissions from geological sources are from a climatology map based on Etiope (2015). The soils uptake is from climatology of Ridgwell et al. (1999).

#### **4 Supplementary Text 4: Wetland emissions from land surface models and wetland extent**

Land surface models estimate CH<sub>4</sub> emissions through a series of processes, including CH<sub>4</sub> production, CH<sub>4</sub> oxidation and transport and are further regulated by the changing environmental factors (Tian et al., 2010; Xu et al., 2010; Melton et al., 2013; Wania et al., 2013; Poulter et al., 2017). In these models, methane emissions from wetlands to the atmosphere are computed as the product of an emission flux density (which can be negative; mass per unit area and unit time) multiplied by a wetland extent; see the model inter-comparison studies by Melton et al. (2013) and Bohn et al. (2015). The CH<sub>4</sub> emission flux density is represented in land surface models with varying levels of complexity (Wania et al. 2013). Many biogeochemical models link CH<sub>4</sub> emissions with net primary production though production of exudates or litter or to soil carbon to yield heterotrophic respiration estimates, although models with more explicit microbial representations of methane production are now being applied (Grant et al., 2019). A proportion of the heterotrophic respiration estimate is then taken to be CH<sub>4</sub> production (Melton et al., 2013), with this proportion calibrated to match regional estimates from aircraft campaigns or global estimates from atmospheric inversions. The oxidation of produced (and becoming atmospheric) methane in the soil column is then either represented explicitly (e.g., Riley et al. (2011), Grant and Roulet (2002)), or fixed proportionally to production (Wania et al., 2013).

In land surface models, wetland extent is either ‘diagnostic’ and prescribed (from inventories or remote sensing data) or ‘prognostic’ and computed numerically (using hydrological models accounting for the fraction of grid cell with flat topography prone to high-water table (e.g., Stocker et al. (2014), Kleinen et al. (2012)). Hybrid approaches can also be implemented with tropical extent prescribed from remote sensing and northern peatland extent explicitly computed (Zhang et al., 2016; Melton et al., 2013). Wetland extent appears to be a primary contributor to uncertainties in methane emissions from wetlands (Bohn et al., 2015, Desai et al., 2015). For instance, the maximum wetland extent on a yearly basis appeared to be very different among prognostic simulations from land surface models (ranging from 7 to 27 Mkm<sup>2</sup>, Melton et al. (2013)), leading to larger uncertainty in derived methane emissions compared to model ensemble using the same prescribed wetland extent from remote sensing observations (Poulter et al., 2017).

Passive and active remote sensing data in the microwave domain have been used to retrieve inundated areas, as with the Global Inundation Extent from Multi-Satellites product (GIEMS, Prigent et al. (2007), Papa et al. (2010)). These remote-sensed data do not exactly correspond to wetlands, as not all flooded areas are wetlands (in the methane emission sense) and some wetlands (e.g. northern bogs) are not always flooded. Inundated areas also include inland water bodies (lakes, ponds, streams, estuaries) and rice paddies, which have to be filtered out to compute wetland emissions. Overall, current remote sensing of wetlands tends to underestimate wetland extent partly because of the spatial resolution of the current satellite passive microwave observations (of the order of 20 km spatial resolution) and partly because microwave signals only detect water above or at the soil surface and therefore do not detect non-inundated, CH<sub>4</sub> emitting peatlands (Prigent et al., 2007). For example, the Global Lakes and Wetlands Dataset (GLWD) (Lehner and Döll, 2004), estimates between 8.2 and 10.1 Mkm<sup>2</sup> of wetlands globally, while remote sensing inundation area is smaller, i.e., ~6 Mkm<sup>2</sup> (Prigent et al., 2007), but with recent estimates up to 30 Mkm<sup>2</sup> (Tootchi et al., 2019).

**Table S1 List of the countries used to define the 18 continental regions**

<b>Region num.</b>	<b>Region name</b>	<b>Countries or territories</b>
1	USA	USA with Alaska, Bermuda Islands
2	Canada	Canada
3	Central America	Anguilla, Antigua and Barbuda, Bahamas, Barbados, Belize, British Virgin Islands, Cayman Islands, Costa Rica, Cuba, Dominica, Dominican Republic, El Salvador, Guadeloupe, Guatemala, Honduras, Jamaica, Martinique, Mexico, Montserrat, Nicaragua, Panama, Puerto Rico, Saint Kitts and Nevis, Saint Lucia, Saint Vincent and the Grenadines, Turks and Caicos Islands, United States Virgin Islands
4	Brazil	Brazil
5	Northern South America	Aruba, Colombia, French Guiana, Grenada, Guyana, , Suriname , Trinidad and Tobago, Venezuela
6	Southwest South America	Argentina, Bolivia, Chile, Ecuador, Peru, Falkland Islands (Malvinas), Paraguay, Uruguay
7	Europe	Albania, Andorra, Austria, Belarus, Belgium, Belgium, Luxembourg, Bulgaria, Channel Islands, Croatia, Cyprus, Czech Republic, Denmark, Estonia, Faroe Islands, Finland, France, Germany, Gibraltar, Greece, Greenland, Hungary, Iceland, Ireland, Isle of Man, Italy, Latvia, Liechtenstein, Lithuania, Luxembourg, Malta, Montenegro, Netherlands, Norway, Poland, Portugal, Republic of Moldova, Romania, Serbia, Slovakia, Slovenia, Spain, Sweden, United Kingdom, Ukraine
8	Northern Africa	Algeria, Cabo Verde, Chad, Côte d'Ivoire, Djibouti, Egypt, Eritrea, Ethiopia, Ethiopia PDR, Gambia, Guinea, Guinea-Bissau, Libya, Mali, Mauritania, Morocco, Saint Helena Ascension and Tristan da Cunha, Sao Tome and Principe, Senegal, Somalia, Sudan former, Tunisia, Western Sahara
9	Equatorial Africa	Benin, Burkina Faso, Burundi, Cameroon, Central African Republic, Congo, Democratic Republic of the Congo, Equatorial Guinea, Gabon, Ghana, Liberia, Nigeria, Rwanda, Sierra Leone, Togo, Uganda, United Republic of Tanzania,
10	Southern Africa	Angola, Botswana, Comoros, Lesotho, Madagascar, Malawi, Mauritius, Mayotte, Mozambique, Namibia, Reunion, Seychelles, South Africa, Swaziland, Zambia, Zimbabwe
11	Russia	Russian federation
12	Central Asia	Kazakhstan, Kyrgyzstan, Tajikistan, Turkmenistan, Uzbekistan, Mongolia,
13	Middle East	Armenia, Azerbaijan, Bahrain, People's Republic of Georgia, Iran, Iraq, Israel, Jordan, Kuwait, Lebanon, Occupied Palestinian Territory, Oman, Qatar, Saudi Arabia, Syrian Arab Republic, Turkey, United Arab Emirates, Yemen
14	China	China mainland, Macao, Hong Kong, Taiwan
15	Korea and Japan	Japan, Korea, Republic of Korea
16	South Asia	Afghanistan, Bangladesh, Bhutan, India, Nepal, Pakistan, Sri Lanka
17	South East Asia	Brunei Darussalam, Cambodia, Guam, Indonesia Kiribati, Lao People's Democratic Republic, Malaysia, Maldives, Marshall Islands, Myanmar, Nauru, Northern Mariana Islands, Palau, Philippines, Singapore, Solomon Islands, Thailand, Timor-Leste, Tokelau, Viet Nam
18	Oceania	American Samoa, Australia, Cook Islands, Fiji, French Polynesia, New Caledonia, New Zealand, Niue, Norfolk Island, Pacific Islands Trust Territory, Papua New Guinea, Pitcairn Islands, Samoa, Tonga, Tuvalu, Vanuatu, Wallis and Futuna Islands

Table S2 Assignment of the inventory specific sectors to GCP sub- and main categories

ESSD Main Category	ESSD Subcategory	EDGARv4.3.2	GAINS by-country	GAINS gridded	CEDS	USEPA
Agriculture and waste	Enteric fermentation and Manure	4A (Enteric fermentation) + 4B (Manure management)	Beef_cattle + Dairy_cows + Sheep_Goats_etc + Pigs + Poultry	Agr (horses, camels) + Agr_buff (buffalo)+ Agr_cow (cows & cattle) + Agr_gosh (sheep & goats) + Agr_pig (pigs)+ Agr_poult (poultry)	3E Enteric Fermentation + 3B_Manure-management	Enteric + manure
	Landfills and Waste	6A + 6D (SWD_LDF Solid waste landfill) + 6C (SWD_INC Solid waste incineration) + 6B (WWT Waste water treatment)	Solid_waste_industry + Solid_waste_municipal + Wastewater_domestic + Wastewater_industry	Wst (wastewater & industrial solid waste) + Wst_MSW (municipal soild waste)	5A_Solid-waste-disposal + 5C_Waste-combustion + 5D_Wastewater-handling + 5E_Other-waste-handling	Landfill + Wastewater + Other waste + Other energy
	Rice	4C + 4D (AGS Agricultural soils)	Rice_cultivation	Agr_fert (rice cultivation)	3D_Rice-Cultivation + 3D_Soil-emissions + 3I_Agriculture-other	Rice
Fossil fuels	Coal	Provided by Greet – I don't think it directly corresponds to any UNFCCC sectors as they are based on use (e.g. electricity generation) rather than fuel type	Coal_mining + Abandoned_coal mines + Powerplant_energy_use_other	MBC (brown coal) + MHC (hard coal)	The split between the Coal, Oil & Gas and Industry sectors is still unclear.	Coal
	Oil & Gas	Provided by Greet (as above) + Residual Oil & Gas* + 7A (FFF Fossil fuel fires) +	Gas_production + Oil_production + Oil_refinery + Powerplant_energy_use_gas	Flr_down (downstream gas flaring) + flr_up (upstream gas flaring) + oth (non-energy gas use) + pp_gas (powerplant gas) + pp_oil (powerplant oil)	The split between the Coal, Oil & Gas and Industry sectors is still unclear	Oil & Gas
	Transport	1A3a_CDS (TNR_Aviation_CDS) + 1A3a CRS (TNR_Aviation_CRS) +	Transport_Domestic_Air + Transport_Other + Transport_Rail +	Air (domestic aviation) + cns (construction machinery) + Rail (Rail) + shp_inw (shipping)	1A3ai_International-aviation + 1A3aii_Domestic-aviation +	Mobile

		1A3a_LTO (TNR_Aviation_LTO + 1A3a_SPS (TNR_Aviation_SPS) + 1A3c + 1A3e (TNR_Other) + 1A3d+ 1C2 (TNR_Ship) + 1A3b (TRO Road transport)	Transport_Road	inland waters) + tra (transport other) + tra_rw_2w (2-wheeled) + tra_rd_hdb (buses) + tra_rd_hdt (trucks) + tra_rd_ld4 (cars) + trc (agriculture machines) +	1A3b_Road + 1A3c_Rail + 1A3di_International- shipping + 1A3di_Oil_tanker_loadi ng + 1A3dii_Domestic- navigation + 1A3eii_Other-transp	
	Industry	2C1a_2C1c_2C1d_2C1e_2C1f_2C 2 (IRO) + 2B (CHE) + 1A1a (ENE) + 1A2 (IND) + 1A1b_1A1c_1A5b1_1B1b_1B2a5 _1B2a6_1B2b5_2C1b (REF_TRF)	Industry_energy_use _gas + Gas_transmission + Industry_energy_use _other + Industry_Brick_kilns	ENE (energy transportation, distribution & conversion losses) + IND (industry energy use) + pp_eng (generator sets)	The split between the Coal, Oil & Gas and Industry sectors is still unclear	Other Ind
Biofuels + Biomass burning	Biofuels + Biomass burning*	1A4 (RCO - Energy for buildings) + Biomass burning*	Domestic_energy_us e_gas + Domestic_energy_us e_firewood + Domestic_energy_us e_other + Biomass burning*	Dom (domestic energy use-combustion) + pp_bio (biomass powerplant) + Biomass burning*	1A4a_Commercial- institutional + 1A4b_Residential + 1A4c_Agriculture- forestry-fishing + Biomass burning*	Biomass + Other Ag

**Table S3 Contributions of the biogeochemical models to the different releases of the global methane budget**

Model Name	Kirschke et al. (2013)	Saunois et al. (2016) Poulter et al. (2017)	This study
CLASS-CTEM	-	Y	Y
CLM4.5	-	Y	-
DLEM	-	Y	Y
ELM	-	-	Y
JSBACH	-	-	Y
JULES	-	Y	Y
LPJ GUESS	-	-	Y
LPJ MPI	-	Y	Y
LPJ-WSL	Y	Y	Y
LPX	Y	Y	Y
ORCHIDEE	Y	Y	Y
SDGVM	-	Y	-
TEM-MDM	-	-	Y
TRIPLEX_GHG	-	Y	Y
VISIT	-	Y	Y
<b>Contributing</b>	3	11	13

Table S4 CCMI models used to estimate OH tropospheric mass-weighted concentrations, methane losses and lifetime. Average over 2000-2010 (Zhao et al., 2019).

	<b>OH tropospheric concentration</b> ( $10^5$ molec cm $^{-3}$ )	<b>Tropospheric methane loss</b> (Tg CH $^4$ yr $^{-1}$ )	<b>Tropospheric<sup>a</sup> methane loss</b> (Tg CH $^4$ yr $^{-1}$ )	<b>Tropospheric methane lifetime<sup>b</sup></b> (years)	<b>Total methane lifetime<sup>c</sup></b> (years)
	<b>Sect 3.3.1</b>	<b>Sect 3.3.1</b>	<b>Sect 3.3.2</b>	<b>Sect. 3.3.5</b>	<b>Sect. 3.3.5</b>
<b>CESM1-CAM4Chem</b>	11.3	506	26	9.5	8.5
<b>CESM1-WACCM</b>	11.4	512	37	9.4	8.2
<b>CMAM</b>	11.3	530	34	9.1	8.0
<b>EMAC-L47MA</b>	11.3	-	-	-	-
<b>EMAC-L90MA</b>	11.5	-	-	-	-
<b>GEOSCCM</b>	12.3	538	36	8.9	7.9
<b>HadGEM3-ES</b>	9.9	-	-	-	-
<b>MOCAGE</b>	12.5	632	12	7.5	7.0
<b>MRI-ESM1r1</b>	10.6	476	36	10.1	8.8
<b>SOCOL3</b>	14.4	677	37	7.2	6.5
<b>UMUKCA-UCAM</b>	11.9	-	-	-	-
<b>Mean</b>		553	31	8.8	7.8
<b>Min</b>		476	12	7.2	6.5
<b>max</b>		677	37	10.1	8.8

<sup>a</sup> tropopause height at 200hPa

<sup>b</sup> defined as total burden divided by tropospheric loss

<sup>c</sup> defined as total burden divided by total loss. Total loss = total chemical loss (tropospheric and stratospheric losses) + 35 Tg from soil uptake

Table S5 Soil uptake estimates from the literature and in this GCP synthesis in Tg CH<sub>4</sub> yr<sup>-1</sup>

Reference	Method	Period	Best estimate	Range	Range explanation
Ridgwell et al. (1999)	Modelling	1990s	38	20-51	Model structural uncertainty
Dutaur and Verchot (2007)	Extrapolation of observations	?	22	10-34	
Curry (2007)	Modelling- CLASS	1979–1999	28	9-47	
Riley et al. (2011)	Modeling - CLM4Me	?	31	15-38	Structural uncertainties
Ito and Inatomi (2012)	Modelling - VISIT	1996-2005		25-35	
Tian et al. (2016)	Modelling - DLEM	2000-2009	30	11-49	
Murguia-Flores et al. (2018)	Modelling – MeMo	2008-2017*	32	29-38	Different parametrizations

\* runs have been performed specifically for this period for this synthesis

Synthesis publications		Mean	Range	Litterature based on
Kirschke et al. (2013)		28	9-47	Curry (2007)
Saunois et al. (2016)		28	9-47	Curry (2007)
This study		30	11- 49	Tian et al. (2016)

**Table S6 Set-up of the different inverse systems contributing to this study.**

		CTE-CH4	GELCA	LMDz-PYVAR	MIRO4-ACTM	NICAM-TM	NIES-TM	TM5-SRON	TM5-JRC	TOMCAT
<b>Main references</b>	Tsuruta et al. (2017)	Ishizawa et al. (2016)	Zheng et al. (2018a, 2018b)	Patra et al. (2018); Watanabe et al. (2008)	Niwa et al. (2017a; 2017b)	Maksyutov et al. (2020); Wang (2019a)	Segers and Houweling (2018, report); Bergamaschi et al. (2010; 2013), Panday et al. (2016)	Bergamaschi et al. (2013, 2018)	McNorton et al. (2018)	
<b>Model characteristics</b>	Meteorology	ECMWF ERA-Interim (Dee et al., 2011)	JRA-55 (Kobayashi et al., 2015)	LMDz nudged to ERA-I	JRA-55 (Kobayashi et al., 2015)	JRA-55 (Kobayashi et al., 2015; Harada et al., 2016)	JCDAS(~2013)/JRA-55(2014~), 6 hourly	ECMWF ERA-Interim, forecasts 3-12 hour, 3 hourly temporal resolution	ECMWF ERA-Interim, forecasts 3-12 hour, 3 hourly temporal resolution	ECMWF ERA-Interim, 6 hourly temporal resolution
	Resolution	Global 6x4 + two-way nested 1x1 zoom over Europe, 25 levels	Coupled NIES-TM (2.5×2.5×32) with FLEXPART v8.0 (1.0×1.0)	(3.75° longitude × 1.9° latitude × 39 layers)	2.8 x 2.8 x 67	~240 km, 40 levels (model top ~45km)	2.5x2.5x32 NIES-TM 0.1x0.1 FLEXPART	3 x 2 x 34	6° x 4° x 25	2.8 x 2.8 x 60

	P B L s c h e m e	Based on parameterisation of Vogelezang and Holtslag (1996) (Krol et al., 2018)	ECMWF ERA-Interim 3 hourly PBL height (NIES-TM)	ECMWF ERA-Interim 6 hourly PBL height	Mellor and Yamada (1974, 1982)	Mellor and Yamada (1974) & Nakanishi and Niino (2004)	ECMWF ERA-Interim 3 hourly PBL height	LTG (Louis, Tiedtke and Geleyn) following Holtslag and Boville (1993)	LTG (Louis, Tiedtke and Geleyn) following Holtslag and Boville (1993)	Holtslag and Boville (1993)
	C o n v e c t i o n S c h e m e	Gregory et al., 2000	Kuo-type scheme following Grell et al. [1995] (NIES-TM)	Tiedtke's scheme	Arakawa and Schubert (1974)	Chikira and Sugiyama (2010)	Tiedtke (1989)	ERA-Interim archived convective fluxes	Tiedtke [1989]	Tiedtke (1989)
I n v e r s i o n s e t -	T i m e r e s o l u t i o n	1 week	monthly	8 days	Monthly	monthly	2 weeks	Monthly	Monthly	Monthly

<b>u p</b>	<b>S p a t i a l r e s o l u t i o n</b>	1x1 over Europe, region-wise elsewhere	43 regions (42 land regions and 1 ocean in the globe)	3.75° longitude × 1.9° latitude	2.8 x 2.8	~240 km	0.1x0.1	3 x 2 x 34	6° x 4°	5 Regional Scaling Factors
<b>P r i o r e r r o r s</b>	80% of flux over land, 20% over ocean	50% for all prior fluxes	70% of prior emissions***	50% of the fluxes over all the basis regions	calculated from the ensemble of VISIT for wetlands, rice cultivation, and soil uptake, and set 30 % for the others	EDGAR 4.2 for anthropogenic (20% of prior), and VISIT for biospheric (50% of prior) emissions	100% for categories wetlands, rice, and biomass burning; 50% for category with remaining sources (mainly anthropogenic)	100% for categories wetlands, rice, and biomass burning; 50% for category with remaining sources (mainly anthropogenic)	50% for all source categories / 2% for OH	
<b>C o r r e l a t i o n l e</b>	500 km over land, 900 km over ocean	-	1000 km (ocean), 500 km (land), 16 days (temporal)***	0 between all the basis regions	calculated from the ensemble of VISIT for wetlands, rice cultivation, and soil uptake, and set 0 km for coal, oil &gas, biomass burnings, and set 500 km for the others	500 km (spatial), 15 days (temporal)	500 km	500 km	-	

	n g t h									
M i n i m i z e r s	Ensemble Kalman filter (Peters et al., 2005)	Kalman Smoother	M1QN3	Bayesian method	POpULar (Fujii and Kamachi, 2003; Fujii, 2005)	VAR (M1QN3; Meirink et al., 2008)	M1QN3	M1QN3	-	
P r i o r s o u r c e s	A n t h r o p o g e n i c	GCP	EDGAR v4.2, climatology (year 2008 emission) after 2008	CEDS***	EDGAR v4.3.2 (Janssens-Maenhout et al. 2017)	GCP	EDGAR v4.3.2	EDGAR v4.2, climatology after 2008	EDGAR v4.3.2 climatology (using 2010)	EDGAR v4.2, extrapolated after 2008

	<b>Biomass burning</b>	GCP	GFED v3.1, GFAS v1.2 after 2011	GFED4.1s	GFEDv4s (van der Werf et al., 2017) and GISS (Fung et al. 1991 )	GCP	GFED (1999-2003), GFAS (2004-2018)	GFED v3.1, climatology after 2011	GFED v4.1	GFED v4, 2015 a repeat of 2014.
	<b>Wetlands</b>	GCP	VISIT (Ito and Inatomi, 2012), climatology (mean for 2009-2013) after 2013	Bloom 2017***	VISIT (Ito and Inatomi, BG, 2013 (revised)	VISIT (Ito and Inatomi, 2012)	VISIT (Ito and Inatomi, 2012), remapped with GLWD to 0.1x0.1 deg	Kaplan climatology	WETCHIMP ensemble mean	JULES modelled emissions from 2003-2014 (2015 repeat of 2014) from McNorton et al. (2016a)
	<b>Rice</b>	GCP	VISIT (Ito and Inatomi, 2012) climatology (mean for 2009-2013) after 2013	CEDS	VISIT (Ito and Inatomi, BG, 2013 (revised)	VISIT (Ito and Inatomi, 2012)	EDGAR v4.3.2	EDGAR v4.2 with Matthews seasonality, climatology after 2008	EDGAR v4.3.2 (2010) with Matthews seasonality	Annually repeating from Yan et al. 2009
	<b>Termites</b>	GCP	GISS, climatology (Fung, I., et al. 1991)	GCP	TransCOM-CH4 (Patra et al., 2011)	GCP	GISS	Sanderson climatology	Sanderson climatology	Termites tomcat 2006 Matthews and Fung 1987)
	<b>Other</b>	GCP		GCP (geological and oceans)	TransCOM-CH4 (Patra et al., 2011)	GCP	Geological: Transcom-CH4 (Patra et al. 2011)	Oceans: Lambert climatology	Oceans: Lambert climatology	Oceans, Hydrates, Geological tomcat 2006

						Oceans: GCP (modified to 0.1x0.1 grid)	Wild animals: Olson climatology	Wild animals: Olson climatology	Matthews and Fung 1987). All emission totals rescaled to Schwietzke et al. (2016) values.	
<b>P r i o r s i n k s</b>	<b>S o l u p t a k e</b>	GCP	VISIT (Ito and Inatomi, 2012)	Ridgwell, 1999	GCP	VISIT (Ito and Inatomi, 2012)	VISIT (Ito and Inatomi, 2012)	Ridgwell climatology	Ridgwell climatology	Patra et al. (2011)
	<b>C h e m i s t r y</b>	OH, (Houweling et al., 2014; Brühl and Crutzen, 1993) Cl, O1D (Bergamaschi et al., 2005)	OH, O(1D), Cl: (Transcom- CH4, Patra et al,2011)	OH, O1D Transcom-CH4 (Patra et al., 2011)	GCP	TransCOM- CH4 (Patra et al., 2011)	OH, O1D, Cl – Transcom-CH4 (Patra et al. 2011)	OH from TM5 (as in Bergamaschi et al., 2010; 2013)  OH, O(1D), Cl stratosphere from ECHAM5- MESSy1 [Bergamaschi et al., 2013]	OH from TM5 (as in Bergamaschi et al., 2010; 2013)  OH, O(1D), Cl stratosphere from ECHAM5- MESSy1 [Bergamaschi et al., 2013]	OH: McNorton et al. (2016b) Tropospheric Cl: Hossaini et al. (2016)
<b>D a t a u s e d i</b>	<b>S u r f a c e</b>	AGAGE, CSIRO, EC, FMI, LSCE, NIES, NOAA, (part of) WDCGG, MPI-BGC, University of Exeter	From WDCGG (NOAA, CSIRO, LSCE, EC, MRI etc) and NIES		NOAA, CSIRO (41 stations)	GCP (AGAGE, CSIRO, EC, FMI, LSCE, NIES, NOAA) & JMA	GCP (AGAGE, CSIRO, EC, FMI, LSCE, NIES, NOAA) & JMA	NOAA	NOAA background stations (discrete air samples only)	NOAA/ESRL for CH4 and NOAA/INSTA AR for d13CH4

<b>n t h e i n v e r s i o n s</b>	<b>S a t e l i t e</b>	NIES L2 retrieval v2.72 (Yoshida et al., 2013)	-	MOPITT v7 CO column (Deeter et al., 2017) OMI HCHO column (González et al., 2015) GOSAT XCH4 (University of Leicester, Parker et al., 2011) ***	-	-	GOSAT NIES L2 retrieval v02.72 (Yoshida et al., 2013)	GOSAT ESA/CCI product v2.3.8 (Detmers & Hasekamp, 2016, report)	GOSAT OCPRv7.2 <a href="https://www.eros.le.ac.uk/data/GHG/GOSAT/v7.2/PUGv4_GHG-CCI_CH4_GOS_OCPR.pdf">https://www.eros.le.ac.uk/data/GHG/GOSAT/v7.2/PUGv4_GHG-CCI_CH4_GOS_OCPR.pdf</a>	-
<b>O b s e r v a t i o n e r r o r s</b>	<b>S u r f a c e o b s e r v a t i o n</b>	4.5 to 75 ppb, depending on sites. No spatial/temporal correlation.	2 to 139 ppb, depending on sites		Variable model error + 5ppb instrumental error	4 ppb multiplied by number of observations within 500 km and half a month	10 to 139 ppb, depending on sites.	Following Bergamaschi et al. (2010)	Following Bergamaschi et al. (2010)	10 ppb / 0.1%

	<b>S a t e l i t e r e r i v e a l</b>	Twice retrieval uncertainty (about 30 ppb)	-	Grid dependent. ~ 150-200 ppb that includes instrument, representation, and forward model errors.	-	-	60 ppb	Combination of GOSAT retrieval error and model representation error. A bias correction is applied when computing the TM5-GOSAT difference, based on the biases between posteriori simulations from the in-situ inversion and the GOSAT product.	based on reported GOSAT retrieval errors; as described in [Bergamaschi et al., 2013] - bias correction as function of latitude and month as described in [Bergamaschi et al., 2013]	-
<b>Time window</b>		1 week	4 months	14 months each year (Nov-Dec)	Monthly	225 months (Jul 1999 – Mar 2018)	18 month each year (Oct-Mar)	Sequence of 3 yearly inversions (2000-2014) or 1 yearly (2015, 2016, 2017), each with 6 months spin-down (as described in [Bergamaschi et al., 2013]).	Sequence of yearly inversions, each with 6 months spin-down (as described in [Bergamaschi et al., 2013]).	Monthly from 2003-2015
<b>Time period covered</b>		Surface : 2000-2017 Satellite: 2010-2017	2000-2015	Surface : 2010-2016 Satellite: 2010-2016/7	2000-2017	Jul99-Mar18	Surface : 2000-2017 Satellite: 2010-2017	Surface : 2000-2017 Satellite: 2010-2017	Surface : 2000-2017 Satellite: 2010-2017	2003-2015

**Table S7 Contributions of the different inverse systems to the different releases of the global methane budget.**

Model Name	Kirschke et al. (2013)	Saunois et al. (2016)	This study
CTE-CH4 (NOAA)	Surface	Surface	-
CTE-CH4 (FMI)	-	-	Surface/GOSAT
GELCA	-	Surface	Surface
GEOSCHEM	Surface	-	-
GISS	Surface	-	-
LMDzPYVAR	Surface	Surface/GOSAT	Surface/GOSAT
LMDz-MIOP	Surface	Surface	-
MATCH	Surface	-	-
MIROC4-ACTM	-	Surface	Surface
NICAM-TM	-	-	Surface
NIESSTM	-	Surface/GOSAT	Surface/GOSAT
TM2	Surface	-	-
TM5-SRON	Surface	Surface/GOSAT	Surface/GOSAT
TM5-JRC	Surface	Surface/GOSAT	Surface/GOSAT
TOMCAT	-	-	Surface
<b>Number of systems Contributing</b>	9	8	9

**Figure S1 Map of the 18 continental regions.** 1: USA; 2: Canada; 3: Central America; 4: Northern South America; 5: Brazil; 6: Southwest Southern America; 7: Europe; 8: Northern Africa; 9: Equatorial Africa; 10: Southern Africa; 11: Russia; 12: Central Asia; 13: Middle East; 14: China; 15: Korea and Japan; 16: South Asia; 17: South East Asia; 18: Oceania.

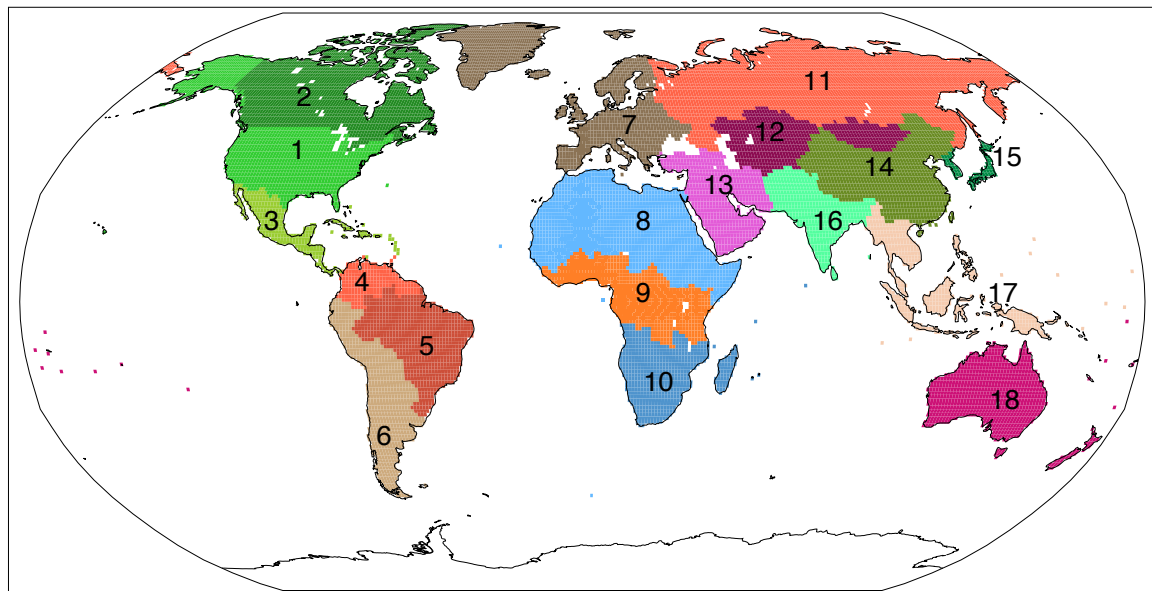
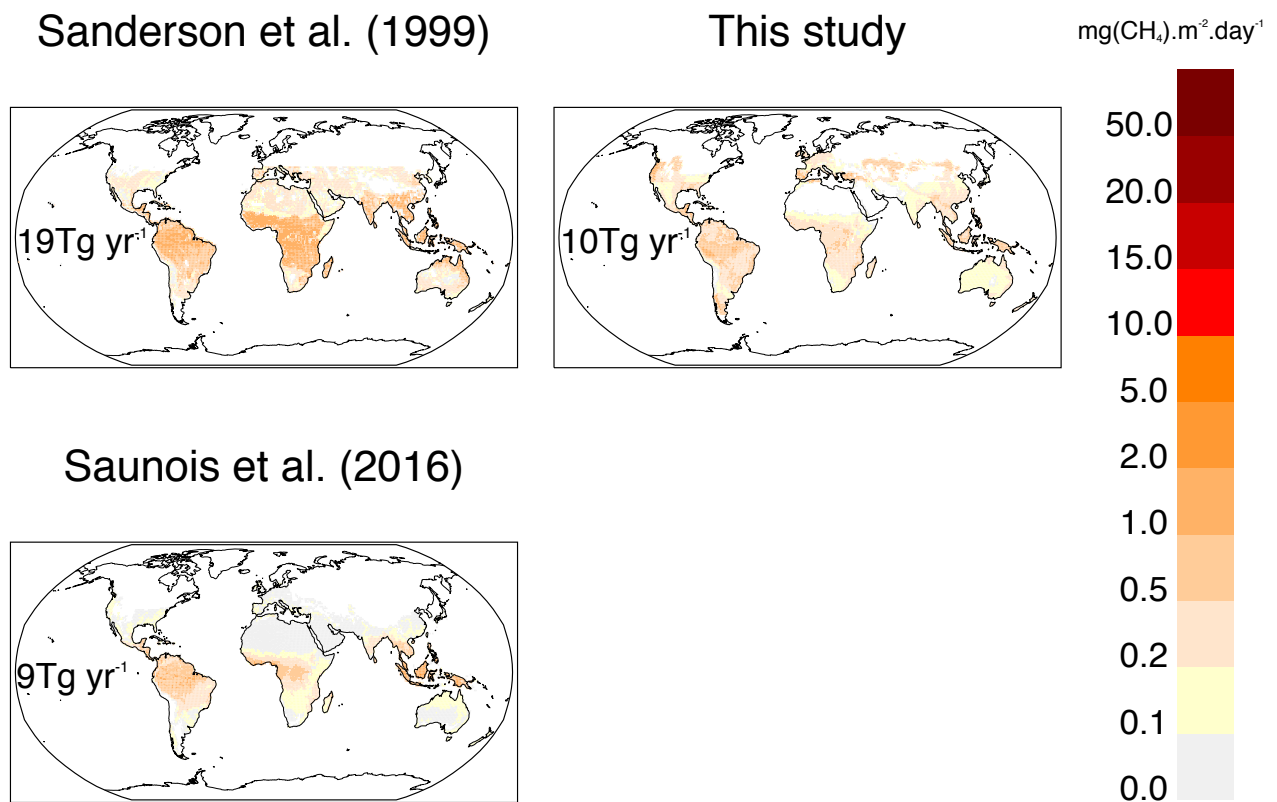


**Figure S2 Comparison of the distribution of methane emissions from termite en mg CH<sub>4</sub> m<sup>-2</sup> day<sup>-1</sup>. Emission distribution from Sanderson et al. (1999), Saunois et al. (2016) and this study. The numbers represent the total annual termite emissions for each distribution.**



## References:

- Alexe, M., Bergamaschi, P., Segers, A., Detmers, R., Butz, A., Hasekamp, O., Guerlet, S., Parker, R., Boesch, H., Frankenberg, C., Scheepmaker, R. A., Dlugokencky, E., Sweeney, C., Wofsy, S. C., and Kort, E. A.: Inverse modelling of CH<sub>4</sub> emissions for 2010–2011 using different satellite retrieval products from GOSAT and SCIAMACHY, *Atmos. Chem. Phys.*, 15, 113-133, doi:10.5194/acp-15-113-2015, 2015
- Andersen, T., Scheeren, B., Peters, W., and Chen, H.: A UAV-based active AirCore system for measurements of greenhouse gases, *Atmos. Meas. Tech.*, 11, 2683-2699, <https://doi.org/10.5194/amt-11-2683-2018>, 2018
- Ars, S., Broquet, G., Yver Kwok, C., Roustan, Y., Wu, L., Arzoumanian, E., and Bousquet, P.: Statistical atmospheric inversion of local gas emissions by coupling the tracer release technique and local-scale transport modelling: a test case with controlled methane emissions, *Atmos. Meas. Tech.*, 10, 5017-5037, <https://doi.org/10.5194/amt-10-5017-2017>, 2017.
- Beck, V., Chen, H., Gerbig, C., Bergamaschi, P., Bruhwiler, L., Houweling, S., Röckmann, T., Kolle, O., Steinbach, J., Koch, T., Sapart, C. J., van der Veen, C., Frankenberg, C., Andreae, M. O., Artaxo, P., Longo, K. M., and Wofsy, S. C.: Methane airborne measurements and comparison to global models during BARCA, *Journal of Geophysical Research: Atmospheres*, 117, D15310, doi:10.1029/2011jd017345, 2012.
- Bergamaschi, P., Frankenberg, C., Meirink, J. F., Krol, M., Dentener, F., Wagner, T., Platt, U., Kaplan, J. O., Koerner, S., Heimann, M., Dlugokencky, E. J., and Goede, A.: Satellite chartography of atmospheric methane from SCIAMACHY on board ENVISAT: 2. Evaluation based on inverse model simulations, *Journal of Geophysical Research-Atmospheres*, 112, D02304, doi:10.1029/2006jd007268, 2007.
- Bergamaschi, P., Frankenberg, C., Meirink, J. F., Krol, M., Villani, M. G., Houweling, S., Dentener, F., Dlugokencky, E. J., Miller, J. B., Gatti, L. V., Engel, A., and Levin, I.: Inverse modeling of global and regional CH<sub>4</sub> emissions using SCIAMACHY satellite retrievals, *Journal of Geophysical Research-Atmospheres*, 114, D22301, doi:10.1029/2009jd012287, 2009.
- Bergamaschi, P., M. Bräunlich, T. Marik, and C.A.M. Brenninkmeijer, Measurements of the carbon and hydrogen isotopes of atmospheric methane at Izana, Tenerife: Seasonal cycles and synoptic-scale variations, *J. Geophys. Res.*, 105 (D11), 14531-14546, 2000.

Bergamaschi, P., Houweling, S., Segers, A., Krol, M., Frankenberg, C., Scheepmaker, R. A., Dlugokencky, E., Wofsy, S. C., Kort, E. A., Sweeney, C., Schuck, T., Brenninkmeijer, C., Chen, H., Beck, V., and Gerbig, C.: Atmospheric CH<sub>4</sub> in the first decade of the 21st century: Inverse modeling analysis using SCIAMACHY satellite retrievals and NOAA surface measurements, *Journal of Geophysical Research: Atmospheres*, 118, 7350-7369, doi:10.1002/jgrd.50480, 2013.

Bohn, T. J., Melton, J. R., Ito, A., Kleinen, T., Spahni, R., Stocker, B. D., Zhang, B., Zhu, X., Schroeder, R., Glagolev, M. V., Maksyutov, S., Brovkin, V., Chen, G., Denisov, S. N., Eliseev, A. V., Gallego-Sala, A., McDonald, K. C., Rawlins, M. A., Riley, W. J., Subin, Z. M., Tian, H., Zhuang, Q., and Kaplan, J. O.: WETCHIMP-WSL: Intercomparison of wetland methane emissions models over West Siberia, *Biogeosciences*, 12, 3321-3349, doi:10.5194/bg-12-3321-2015, 2015.

Bousquet, P., Ciais, P., Miller, J. B., Dlugokencky, E. J., Hauglustaine, D. A., Prigent, C., Van der Werf, G. R., Peylin, P., Brunke, E. G., Carouge, C., Langenfelds, R. L., Lathiere, J., Papa, F., Ramonet, M., Schmidt, M., Steele, L. P., Tyler, S. C., and White, J.: Contribution of anthropogenic and natural sources to atmospheric methane variability, *Nature*, 443, 439-443, 2006.

Buchwitz, M., de Beek, R., Noel, S., Burrows, J. P., Bovensmann, H., Schneising, O., Khlystova, I., Bruns, M., Bremer, H., Bergamaschi, P., Korner, S., and Heimann, M.: Atmospheric carbon gases retrieved from SCIAMACHY by WFM-DOAS: version 0.5 CO and CH<sub>4</sub> and impact of calibration improvements on CO<sub>2</sub> retrieval, *Atmospheric Chemistry and Physics*, 6, 2727-2751, 2006.

Burrows, J. P., Höhlzle, B., Goede, A. P. H., Visser, H., and Fricke, W.: SCIAMACHY - Scanning Imaging Absorption Spectrometer for Atmospheric Chartography, *Acta Astr.*, 35, 445-451, 1995.

Butz, A., Guerlet, S., Hasekamp, O., Schepers, D., Galli, A., Aben, I., Frankenberg, C., Hartmann, J. M., Tran, H., Kuze, A., Keppel-Aleks, G., Toon, G., Wunch, D., Wennberg, P., Deutscher, N., Griffith, D., Macatangay, R., Messerschmidt, J., Notholt, J., and Warneke, T.: Toward accurate CO<sub>2</sub> and CH<sub>4</sub> observations from GOSAT, *Geophysical Research Letters*, 38, L14812, doi:10.1029/2011gl047888, 2011.

Chang, R. Y.-W., Miller, C. E., Dinardo, S. J., Karion, A., Sweeney, C., Daube, B. C., Henderson, J. M., Mountain, M. E., Eluszkiewicz, J., Miller, J. B., Bruhwiler, L. M. P., and Wofsy, S. C.:

Methane emissions from Alaska in 2012 from CARVE airborne observations, Proceedings of the National Academy of Sciences, 111, 16694-16699, doi:10.1073/pnas.1412953111, 2014.

Chen, Y. H., and Prinn, R. G.: Estimation of atmospheric methane emissions between 1996 and 2001 using a three-dimensional global chemical transport model, Journal of Geophysical Research-Atmospheres, 111, D10307, doi:10.1029/2005JD006058, 2006.

Chevallier, F., Fisher, M., Peylin, P., Serrar, S., Bousquet, P., Breon, F. M., Chedin, A., and Ciais, P.: Inferring CO<sub>2</sub> sources and sinks from satellite observations: Method and application to TOVS data, Journal of Geophysical Research-Atmospheres, 110, D24309, doi:10.1029/2005jd006390, 2005.

Chevallier, F., Bréon, F. M., and Rayner, P. J.: Contribution of the Orbiting Carbon Observatory to the estimation of CO<sub>2</sub> sources and sinks: Theoretical study in a variational data assimilation framework, J Geophys Res-Atmos, 112, D09307, 10.1029/2006jd007375, 2007.

Cressot, C., Chevallier, F., Bousquet, P., Crevoisier, C., Dlugokencky, E. J., Fortems-Cheiney, A., Frankenberg, C., Parker, R., Pison, I., Scheepmaker, R. A., Montzka, S. A., Krummel, P. B., Steele, L. P., and Langenfelds, R. L.: On the consistency between global and regional methane emissions inferred from SCIAMACHY, TANSO-FTS, IASI and surface measurements, Atmospheric Chemistry and Physics, 14, 577-592, doi:10.5194/acp-14-577-2014, 2014.

Crevoisier, C., Nobileau, D., Fiore, A. M., Armante, R., Chedin, A., and Scott, N. A.: Tropospheric methane in the tropics - first year from IASI hyperspectral infrared observations, Atmospheric Chemistry and Physics, 9, 6337-6350, 2009.

Desai, A. R., Xu, K., Tian, H., Weishampel, P., Thom, J., Baumann, D., Andrews, A. E., Cook, B. D., King, J. Y., and Kolka, R.: Landscape-level terrestrial methane flux observed from a very tall tower, Agricultural and Forest Meteorology, 201, 61-75, doi:10.1016/j.agrformet.2014.10.017 2015

Dils, B., De Mazière, M., Müller, J. F., Blumenstock, T., Buchwitz, M., de Beek, R., Demoulin, P., Duchatelet, P., Fast, H., Frankenberg, C., Gloudemans, A., Griffith, D., Jones, N., Kerzenmacher, T., Kramer, I., Mahieu, E., Mellqvist, J., Mittermeier, R. L., Notholt, J., Rinsland, C. P., Schrijver, H., Smale, D., Strandberg, A., Straume, A. G., Stremme, W., Strong, K., Sussmann, R., Taylor, J., van den Broek, M., Velazco, V., Wagner, T., Warneke, T., Wiacek, A., and Wood, S.: Comparisons between SCIAMACHY and ground-based FTIR data for total columns of CO, CH<sub>4</sub>, CO<sub>2</sub> and N<sub>2</sub>O, Atmospheric Chemistry and Physics, 6, 1953-1976, doi:10.5194/acp-6-1953-2006, 2006.

Etiope, G.: Natural Gas Seepage. The Earth's Hydrocarbon Degassing, Springer International Publishing, 199 pp., doi:10.1007/978-3-319-14601-0, 2015.

Fisher, R. E., Sriskantharajah, S., Lowry, D., Lanoiselle, M., Fowler, C. M. R., James, R. H., Hermansen, O., Myhre, C. L., Stohl, A., Greinert, J., Nisbet-Jones, P. B. R., Mienert, J., and Nisbet, E. G.: Arctic methane sources: Isotopic evidence for atmospheric inputs, *Geophysical Research Letters*, 38, L21803, doi:10.1029/2011gl049319, 2011.

Frankenberg, C., Aben, I., Bergamaschi, P., Dlugokencky, E. J., van Hees, R., Houweling, S., van der Meer, P., Snel, R., and Tol, P.: Global column-averaged methane mixing ratios from 2003 to 2009 as derived from SCIAMACHY: Trends and variability, *Journal of Geophysical Research-Atmospheres*, 116, D04302, doi:10.1029/2010jd014849, 2011.

Gatti, L. V., Gloor, M., Miller, J. B., Doughty, C. E., Malhi, Y., Domingues, L. G., Basso, L. S., Martinewski, A., Correia, C. S. C., Borges, V. F., Freitas, S., Braz, R., Anderson, L. O., Rocha, H., Grace, J., Phillips, O. L., and Lloyd, J.: Drought sensitivity of Amazonian carbon balance revealed by atmospheric measurements, *Nature*, 506, 76-80, doi:10.1038/nature12957, 2014.

Grant, R. F., Z. A. Mekonnen, and W. J. Riley: Climate change impacts on CO<sub>2</sub> and CH<sub>4</sub> exchange in an Arctic polygonal tundra depend on changes in vegetation and drainage, *JGR-Biogeosciences*, doi: 10.1029/2018JG004645, 2019

Grant, R. F., and Roulet, N. T.: Methane efflux from boreal wetlands: Theory and testing of the ecosystem model Ecosys with chamber and tower flux measurements, *Global Biogeochemical Cycles*, 16, 2-1-2-16, 10.1029/2001gb001702, 2002.

Gvakharia, A., Kort, E. A., Brandt, A., Peischl, J., Ryerson, T. B., Schwarz, J. P., Smith, M. L. and Sweeney, C.: Methane, Black Carbon, and Ethane Emissions from Natural Gas Flares in the Bakken Shale, North Dakota, *Environmental Science & Technology*, 51, 5317-5325, DOI: 10.1021/acs.est.6b05183, 2017

Hein, R., Crutzen, P. J., and Heimann, M.: An inverse modeling approach to investigate the global atmospheric methane cycle, *Global Biogeochemical Cycles*, 11, 43-76, 1997.

Houweling, S., Krol, M., Bergamaschi, P., Frankenberg, C., Dlugokencky, E. J., Morino, I., Notholt, J., Sherlock, V., Wunch, D., Beck, V., Gerbig, C., Chen, H., Kort, E. A., Röckmann, T., and Aben, I.: A multi-year methane inversion using SCIAMACHY, accounting for systematic errors using TCCON measurements, *Atmospheric Chemistry and Physics*, 14, 3991-4012, doi:10.5194/acp-14-3991-2014, 2014.

Janssens-Maenhout, G., Crippa, M., Guizzardi, D., Muntean, M., Schaaf, E., Dentener, F., Bergamaschi, P., Pagliari, V., Olivier, J., Peters, J., van Aardenne, J., Monni, S., Doering, U., Petrescu, R., Solazzo, E., and Oreggioni, G.: EDGAR v4.3.2 Global Atlas of the three major Greenhouse Gas Emissions for the period 1970-2012, *Earth Syst. Sci. Data Discuss.*, 2019, 1-52, doi:10.5194/essd-2018-164, 2019.

Joly, L., Robert, C., Parvitte, B., Catoire, V., Durry, G., Richard, G., Nicoullaud, B., and Zéninari, V.: Development of a spectrometer using a cw DFB quantum cascade laser operating at room temperature for the simultaneous analysis of N<sub>2</sub>O and CH<sub>4</sub> in the Earth's atmosphere *Applied Optics*, 47, 1206-1214, 2008.

Kaminski, T., Rayner, P. J., Heimann, M., and Enting, I. G.: On aggregation errors in atmospheric transport inversions, *Journal of Geophysical Research-Atmospheres*, 106, 4703-4715, 2001.

Karion, A., Sweeney, C., Tans, P., and Newberger, T.: AirCore: An Innovative Atmospheric Sampling System, *Journal of Atmospheric and Oceanic Technology* 27, 1839-1853 2010.

Karion, A., Sweeney, C., Kort, E. A., Shepson, P. B., Brewer, A., Cambaliza, M., Conley, S. A., Davis, K., Deng, A., Hardesty, M., Herndon, S. C., Lauvaux, T., Lavoie, T., Lyon, D., Newberger, T., Pétron, G., Rella, C., Smith, M., Wolter, S.? Yacovitch, T. I., and Tans, P.: Aircraft-Based Estimate of Total Methane Emissions from the Barnett Shale Region, *Environmental Science & Technology* 2015 49 (13), 8124-8131, DOI: 10.1021/acs.est.5b00217, 2015

Kirschke, S., Bousquet, P., Ciais, P., Saunois, M., Canadell, J. G., Dlugokencky, E. J., Bergamaschi, P., Bergmann, D., Blake, D. R., Bruhwiler, L., Cameron-Smith, P., Castaldi, S., Chevallier, F., Feng, L., Fraser, A., Heimann, M., Hodson, E. L., Houweling, S., Josse, B., Fraser, P. J., Krummel, P. B., Lamarque, J. F., Langenfelds, R. L., Le Quere, C., Naik, V., O'Doherty, S., Palmer, P. I., Pison, I., Plummer, D., Poulter, B., Prinn, R. G., Rigby, M., Ringeval, B., Santini, M., Schmidt, M., Shindell, D. T., Simpson, I. J., Spahni, R., Steele, L. P., Strode, S. A., Sudo, K., Szopa, S., van der Werf, G. R., Voulgarakis, A., van Weele, M., Weiss, R. F., Williams, J. E., and Zeng, G.: Three decades of global methane sources and sinks, *Nature Geoscience*, 6, 813-823, doi:10.1038/ngeo1955, 2013.

Kleinen, T., Brovkin, V., and Schuldt, R. J.: A dynamic model of wetland extent and peat accumulation: results for the Holocene, *Biogeosciences*, 9, 235-248, doi:10.5194/bg-9-235-2012, 2012.

Lambert, G., and Schmidt, S.: Reevaluation of the oceanic flux of methane: Uncertainties and long term variations, *Chemosphere*, 26, 579-589, doi:10.1016/0045-6535(93)90443-9., 1993.

Lassey, K. R., Etheridge, D. M., Lowe, D. C., Smith, A. M., and Ferretti, D. F.: Centennial evolution of the atmospheric methane budget: what do the carbon isotopes tell us?, *Atmospheric Chemistry and Physics*, 7, 2119-2139, 2007a.

Lehner, B., and Döll, P.: Development and validation of a global database of lakes, reservoirs and wetlands, *Journal of Hydrology*, 296, 1-22, doi:10.1016/j.jhydrol.2004.03.028, 2004.

Lowe, D. C., Brenninkmeijer, C. A. M., Manning, M. R., Sparks, R., and Wallace, G.: Radiocarbon determination of atmospheric methane at Baring Head, New Zealand, *Nature*, 332, 522-525, 1988.

Lowe, D. C., Brenninkmeijer, C. A. M., Brailsford, G. W., Lassey, K. R., Gomez, A. J., and Nisbet, E. G.: Concentration and  $^{13}\text{C}$  records of atmospheric methane in New Zealand and Antarctica: Evidence for changes in methane sources, *Journal of Geophysical Research: Atmospheres*, 99, 16913-16925, doi:10.1029/94jd00908, 1994.

Machida, T., Matsueda, H., Sawa, Y., Nakagawa, Y., Hirotani, K., Kondo, N., Goto, K., Nakazawa, T., Ishikawa, K., and Ogawa, T.: Worldwide measurements of atmospheric CO<sub>2</sub> and other trace gas species using commercial airlines, *Journal Atmospheric and Oceanic Technoogy*, 25, 1744-1754, doi:10.1175/2008JTECHA1082.1, 2008.

McCalley, C. K., Woodcroft, B. J., Hodgkins, S. B., Wehr, R. A., Kim, E.-H., Mondav, R., Crill, P. M., Chanton, J. P., Rich, V. I., Tyson, G. W., and Saleska, S. R.: Methane dynamics regulated by microbial community response to permafrost thaw, *Nature*, 514, 478-481, doi:10.1038/nature13798, 2014.

McManus, J. B., Nelson, D. D., and Zahniser, M. S.: Long-term continuous sampling of  $^{12}\text{CO}_2$ ,  $^{13}\text{CO}_2$  and  $^{12}\text{C}^{18}\text{O}^{16}\text{O}$  in ambient air with a quantum cascade laser spectrometer, *Isotopes in Environmental and Health Studies*, 46, 49-63, doi:10.1080/10256011003661326, 2010.

McNorton, J., Wilson, C., Gloor, M., Parker, R. J., Boesch, H., Feng, W., Hossaini, R., and Chipperfield, M. P.: Attribution of recent increases in atmospheric methane through 3-D inverse modelling, *Atmos. Chem. Phys.*, 18, 18149-18168, <https://doi.org/10.5194/acp-18-18149-2018>, 2018.

Meirink, J. F., Bergamaschi, P., Frankenberg, C., d'Amelio, M. T. S., Dlugokencky, E. J., Gatti, L. V., Houweling, S., Miller, J. B., Rockmann, T., Villani, M. G., and Krol, M. C.: Four-

dimensional variational data assimilation for inverse modeling of atmospheric methane emissions: Analysis of SCIAMACHY observations, *Journal of Geophysical Research-Atmospheres*, 113, D17301, 2008a.

Meirink, J. F., Bergamaschi, P., and Krol, M. C.: Four-dimensional variational data assimilation for inverse modelling of atmospheric methane emissions: method and comparison with synthesis inversion, *Atmospheric Chemistry and Physics*, 8, 6341-6353, 2008b.

Melton, J. R., Schaefer, H., and Whiticar, M. J.: Enrichment in  $^{13}\text{C}$  of atmospheric CH<sub>4</sub> during the Younger Dryas termination, *Climate of the Past*, 8, 1177-1197, doi:10.5194/cp-8-1177-2012, 2012.

Melton, J. R., Wania, R., Hodson, E. L., Poulter, B., Ringeval, B., Spahni, R., Bohn, T., Avis, C. A., Beerling, D. J., Chen, G., Eliseev, A. V., Denisov, S. N., Hopcroft, P. O., Lettenmaier, D. P., Riley, W. J., Singarayer, J. S., Subin, Z. M., Tian, H., Zürcher, S., Brovkin, V., van Bodegom, P. M., Kleinen, T., Yu, Z. C., and Kaplan, J. O.: Present state of global wetland extent and wetland methane modelling: conclusions from a model intercomparison project (WETCHIMP), *Biogeosciences*, 10, 753-788, doi:10.5194/bg-10-753-2013, 2013.

Membrive, O., Crevoisier, C., Sweeney, C., Danis, F., Hertzog, A., Engel, A., Bönisch, H., and Picon, L.: AirCore-HR: a high-resolution column sampling to enhance the vertical description of CH<sub>4</sub> and CO<sub>2</sub>, *Atmos. Meas. Tech.*, 10, 2163-2181, <https://doi.org/10.5194/amt-10-2163-2017>, 2017.

Mikaloff Fletcher, S. E. M., Tans, P. P., Bruhwiler, L. M., Miller, J. B., and Heimann, M.: CH<sub>4</sub> sources estimated from atmospheric observations of CH<sub>4</sub> and its  $^{13}\text{C}/^{12}\text{C}$  isotopic ratios: 1. Inverse modeling of source processes, *Global Biogeochemical Cycles*, 18, GB4004, doi:10.1029/2004GB002223, 2004.

Milkov, A. V. and Etiope, G.: Revised genetic diagrams for natural gases based on a global dataset of >20,000 samples, *Organic Geochemistry*, 125, 109-120, doi:10.1016/j.orggeochem.2018.09.002, 2018

Miller, J. B., Mack, K. A., Dissly, R., White, J. W. C., Dlugokencky, E. J., and Tans, P. P.: Development of analytical methods and measurements of  $^{13}\text{C}/^{12}\text{C}$  in atmospheric CH<sub>4</sub> from the NOAA Climate Monitoring and Diagnostics Laboratory Global Air Sampling Network, *Journal of Geophysical Research: Atmospheres*, 107, 4178, doi:10.1029/2001jd000630, 2002.

Monteil, G., Houweling, S., Dlugokenky, E. J., Maenhout, G., Vaughn, B. H., White, J. W. C., and Rockmann, T.: Interpreting methane variations in the past two decades using measurements of CH<sub>4</sub> mixing ratio and isotopic composition, *Atmospheric Chemistry and Physics*, 11, 9141-9153, doi:10.5194/acp-11-9141-2011, 2011.

Morino, I., Uchino, O., Inoue, M., Yoshida, Y., Wennberg, P. O., Toon, G. C., Wunch, D., Roehl, C. M., Notholt, J., Warneke, T., Messerschmidt, J., Griffith, D. W. T., Deutscher, N. M., Sherlock, V., Connor, B., Robinson, J., Sussmann, R. and Rettinger, M.: Preliminary validation of column-averaged volume mixing ratios of carbon dioxide and methane retrieved from GOSAT short-wavelength infrared spectra. *Atmospheric Measurement Techniques*, 4 (6), 1061-1076, 2011

Morimoto, S., Aoki, S., Nakazawa, T., and Yamanouchi, T.: Temporal variations of the carbon isotopic ratio of atmospheric methane observed at Ny Ålesund, Svalbard from 1996 to 2004, *Geophysical Research Letters*, 33, L01807, doi:10.1029/2005gl024648, 2006.

Neef, L., van Weele, M., and van Velthoven, P.: Optimal estimation of the present-day global methane budget, *Global Biogeochemical Cycles*, 24, GB0424, doi:10.1029/2009GB003661, 2010.

Papa, F., Prigent, C., Aires, F., Jimenez, C., Rossow, W. B., and Matthews, E.: Interannual variability of surface water extent at the global scale, 1993-2004, *Journal of Geophysical Research*, 115, D12111, doi:10.1029/2009jd012674, 2010.

Paris, J.-D., Ciais, P., Nedelec, P., Stohl, A., Belan, B. D., Arshinov, M. Y., Carouge, C., Golitsyn, G. S., and Granberg, I. G.: New insights on the chemical composition of the Siberian air shed from the YAK AEROSIB aircraft campaigns, *Bulletin of the American Meteorological Society*, 91, 625-641, doi:10.1175/2009BAMS2663.1., 2010.

Peischl, J., et al.: Quantifying atmospheric methane emissions from oil and natural gas production in the Bakken shale region of North Dakota, *J. Geophys. Res. Atmos.*, 121, 6101– 6111, doi:10.1002/2015JD024631, 2016

Poulter, B., Bousquet, P., Canadell, J. G., Ciais, P., Peregon, A., Saunois, M., Arora, V. K., Beerling, D. J., Brovkin, V., Jones, C. D., Joos, F., Gedney, N., Ito, A., Kleinen, T., Koven, C. D., McDonald, K., Melton, J. R., Peng, C. H., Peng, S. S., Prigent, C., Schroeder, R., Riley, W. J., Saito, M., Spahni, R., Tian, H. Q., Taylor, L., Viovy, N., Wilton, D., Wiltshire, A., Xu, X. Y., Zhang, B. W., Zhang, Z., and Zhu, Q. A.: Global wetland contribution to 2000-2012

atmospheric methane growth rate dynamics, Environmental Research Letters, 12, 10.1088/1748-9326/aa8391, 2017.

Prigent, C., Papa, F., Aires, F., Rossow, W. B., and Matthews, E.: Global inundation dynamics inferred from multiple satellite observations, 1993-2000, Journal of Geophysical Research-Atmospheres, 112, D12107, doi:10.1029/2006JD007847, 2007.

Quay, P. D., King, S. L., Stutsman, J., Wilbur, D. O., Steele, L. P., Fung, I., Gammon, R. H., Brown, T. A., Farwell, G. W., Grootes, P. M., and Schmidt, F. H.: Carbon isotopic composition of atmospheric CH<sub>4</sub>: fossil and biomass burning source strengths, Global Biogeochemical Cycles, 5, 25-47, 1991.

Quay, P., Stutsman, J., Wilbur, D., Snover, A., Dlugokencky, E., and Brown, T.: The isotopic composition of atmospheric methane, Global Biogeochemical Cycles, 13, 445-461, 1999.

Rice, A. L., Gotoh, A. A., Ajie, H. O., and Tyler, S. C.: High-Precision Continuous-Flow Measurement of δ<sup>13</sup>C and δD of Atmospheric CH<sub>4</sub>, Analytical Chemistry, 73, 4104-4110, doi:10.1021/ac0155106, 2001.

Rice, A. L., Butenhoff, C. L., Team, D. G., Röger, F. H., Khalil, M. A. K., and Rasmussen, R. A.: Atmospheric methane isotopic record favors fossil sources flat in 1980s and 1990s with recent increase, Proceedings of the National Academy of Sciences, doi:201522923, 10.1073/pnas.1522923113, 2016.

Ridgwell, A. J., Marshall, S. J., and Gregson, K.: Consumption of atmospheric methane by soils: A process-based model, Global Biogeochemical Cycles, 13, 59-70, doi:10.1029/1998gb900004, 1999.

Rigby, M., Manning, A. J., and Prinn, R. G.: The value of high-frequency, high-precision methane isotopologue measurements for source and sink estimation, Journal of Geophysical Research-Atmospheres, 117, D12312, doi:10.1029/2011jd017384, 2012.

Rigby, M., Montzka, S. A., Prinn, R. G., White, J. W. C., Young, D., O'Doherty, S., Lunt, M. F., Ganesan, A. L., Manning, A. J., Simmonds, P. G., Salameh, P. K., Harth, C. M., Mühle, J., Weiss, R. F., Fraser, P. J., Steele, L. P., Krumbel, P. B., McCulloch, A., and Park, S.: Role of atmospheric oxidation in recent methane growth, Proceedings of the National Academy of Sciences, 114, 5373, 2017.

Riley, W. J., Subin, Z. M., Lawrence, D. M., Swenson, S. C., Torn, M. S., Meng, L., Mahowald, N. M., and Hess, P.: Barriers to predicting changes in global terrestrial methane fluxes: analyses

using CLM4Me, a methane biogeochemistry model integrated in CESM, *Biogeosciences*, 8, 1925-1953, doi:10.5194/bg-8-1925-2011, 2011.

Röckmann, T., Brass, M., Borchers, R., and Engel, A.: The isotopic composition of methane in the stratosphere: high-altitude balloon sample measurements, *Atmospheric Chemistry and Physics*, 11, 13,287-213,304, doi:10.5194/acp-11-13287-2011, 2011.

Röckmann, T., Eyer, S., van der Veen, C., Popa, M. E., Tuzson, B., Monteil, G., Houweling, S., Harris, E., Brunner, D., Fischer, H., Zazzeri, G., Lowry, D., Nisbet, E. G., Brand, W. A., Necki, J. M., Emmenegger, L., and Mohn, J.: In situ observations of the isotopic composition of methane at the Cabauw tall tower site, *Atmos. Chem. Phys.*, 16, 10469-10487, <https://doi.org/10.5194/acp-16-10469-2016>, 2016.

Rodgers, C. D.: Inverse methods for atmospheric sounding: theory and practice, *Atmospheric, Oceanic and Planetary Physics*, edited by: World-Scientific, Singapore, London, 240 pp., 2000.

Santoni, G. W., Lee, B. H., Goodrich, J. P., Varner, R. K., Crill, P. M., McManus, J. B., Nelson, D. D., Zahniser, M. S., and Wofsy, S. C.: Mass fluxes and isofluxes of methane ( $\text{CH}_4$ ) at a New Hampshire fen measured by a continuous wave quantum cascade laser spectrometer, *Journal of Geophysical Research: Atmospheres*, 117, D10301, doi:10.1029/2011jd016960, 2012.

Schaefer, H., Fletcher, S. E. M., Veidt, C., Lassey, K. R., Brailsford, G. W., Bromley, T. M., Dlugokencky, E. J., Michel, S. E., Miller, J. B., Levin, I., Lowe, D. C., Martin, R. J., Vaughn, B. H., and White, J. W. C.: A 21st century shift from fossil-fuel to biogenic methane emissions indicated by  $^{13}\text{CH}_4$ , *Science*, 352, 80-84, doi:10.1126/science.aad2705, 2016.

Schuck, T. J., Ishijima, K., Patra, P. K., Baker, A. K., Machida, T., Matsueda, H., Sawa, Y., Umezawa, T., Brenninkmeijer, C. A. M., and Lelieveld, J.: Distribution of methane in the tropical upper troposphere measured by CARIBIC and CONTRAIL aircraft, *Journal of Geophysical Research: Atmospheres*, 117, D19304, doi:10.1029/2012jd018199, 2012.

Schwietzke, S., Sherwood, O. A., Bruhwiler, L. M. P., Miller, J. B., Etiope, G., Dlugokencky, E. J., Michel, S. E., Arling, V. A., Vaughn, B. H., White, J. W. C. and Tans, P. P.: Upward revision of global fossil fuel methane emissions based on isotope database, *Nature*, 538,88-91, doi: 10.1038/nature19797, 2016.

Stocker, B. D., Spahni, R., and Joos, F.: DYPTOP: a cost-efficient TOPMODEL implementation to simulate sub-grid spatio-temporal dynamics of global wetlands and peatlands, *Geoscientific Model Development*, 7, 3089-3110, doi:10.5194/gmd-7-3089-2014, 2014.

Sweeney, C., Karion, A., Wolter, S., Newberger, T., Guenther, D., Higgs, J. A., Andrews, A. E., Lang, P. M., Neff, D., Dlugokencky, E., Miller, J. B., Montzka, S. A., Miller, B. R., Masarie, K. A., Biraud, S. C., Novelli, P. C., Crotwell, M., Crotwell, A. M., Thoning, K., and Tans, P. P.: Seasonal climatology of CO<sub>2</sub> across North America from aircraft measurements in the NOAA/ESRL Global Greenhouse Gas Reference Network, *Journal of Geophysical Research: Atmospheres*, 120, 5155-5190, doi:10.1002/2014jd022591, 2015.

Tarantola, A.: Inverse problem theory, edited by: Elsevier, Amsterdam, The Netherlands, 1987.

Thompson, R. L., Stohl, A., Zhou, L. X., Dlugokencky, E., Fukuyama, Y., Thojima, Y., Kim, S.-Y., Lee, H., Nisbet, E.G., Fisher, R.E., Lowry, D., Weiss, R. F., Prinn, R.G., O'Doherty, S., Young, D., and White, J. W. C.: Methane emissions in East Asia for 2000–2011 estimated using an atmospheric Bayesian inversion, *Journal of Geophysical Research Atmosphere*, 120, 4352–4369. doi:10.1002/2014JD022394, 2015.

Thompson, R. L., Nisbet, E. G., Pisso, I., Stohl, A., Blake, D., Dlugokencky, E. J., Helmig, D., and White, J. W. C.: Variability in Atmospheric Methane From Fossil Fuel and Microbial Sources Over the Last Three Decades, *Geophysical Research Letters*, 45, 11,499-411,508, doi:10.1029/2018GL078127, 2018.

Tian, H., Xu, X., Liu, M., Ren, W., Zhang, C., Chen, G., and Lu, C.: Spatial and temporal patterns of CH<sub>4</sub> and N<sub>2</sub>O fluxes in terrestrial ecosystems of North America during 1979–2008: application of a global biogeochemistry model, *Biogeosciences*, 7, 2673-2694, doi:10.5194/bg-7-2673-2010, 2010.

Tootchi, A., Jost, A., and Ducharne, A.: Multi-source global wetland maps combining surface water imagery and groundwater constraints, *Earth Syst. Sci. Data*, 11, 189-220, <https://doi.org/10.5194/essd-11-189-2019>, 2019.

Turner, A. J., Frankenberg, C., Wennberg, P. O., and Jacob, D. J.: Ambiguity in the causes for decadal trends in atmospheric methane and hydroxyl, *Proceedings of the National Academy of Sciences*, doi: 10.1073/pnas.1616020114, 2017.

Tyler, S. C., Rice, A. L., and Ajie, H. O.: Stable isotope ratios in atmospheric CH<sub>4</sub>: Implications for seasonal sources and sinks, *Journal of Geophysical Research-Atmospheres*, 112, D03303, doi:10.1029/2006JD007231, 2007.

Umezawa, T., Goto, D., Aoki, S., Ishijima, K., Patra, P. K., Sugawara, S., Morimoto, S., and Nakazawa, T.: Variations of tropospheric methane over Japan during 1988–2010, Tellus, B66, 23837, doi:10.3402/tellusb.v66.23837, 2014.

Umezawa, T., Machida, T., Aoki, S., and Nakazawa, T.: Contributions of natural and anthropogenic sources to atmospheric methane variations over western Siberia estimated from its carbon and hydrogen isotopes, Global Biogeochemical Cycles, 26, GB4009, doi:10.1029/2011gb004232, 2012.

Wania, R., Melton, J. R., Hodson, E. L., Poulter, B., Ringeval, B., Spahni, R., Bohn, T., Avis, C. A., Chen, G., Eliseev, A. V., Hopcroft, P. O., Riley, W. J., Subin, Z. M., Tian, H., van Bodegom, P. M., Kleinen, T., Yu, Z. C., Singarayer, J. S., Zurcher, S., Lettenmaier, D. P., Beerling, D. J., Denisov, S. N., Prigent, C., Papa, F., and Kaplan, J. O.: Present state of global wetland extent and wetland methane modelling: Methodology of a model inter-comparison project (WETCHIMP), Geoscientific Model Development, 6, 617-641, doi:10.5194/gmd-6-617-2013, 2013.

Wilson, C., Gloor, M., Gatti, L. V., Miller, J. B., Monks, S. A., McNorton, J., Bloom, A. A., Basso, L. S., and Chipperfield, M. P.: Contribution of regional sources to atmospheric methane over the Amazon Basin in 2010 and 2011, Global Biogeochem. Cycles, 30, 400– 420, doi:10.1002/2015GB005300, 2016

Wofsy, S. C.: HIAPER Pole-to-Pole Observations (HIPPO): fine-grained, global-scale measurements of climatically important atmospheric gases and aerosols, Philosophical Transactions of the Royal Society of London A: Mathematical, Physical and Engineering Sciences, 369, 2073-2086, doi:10.1098/rsta.2010.0313, 2011.

Wunch, D., Toon, G., Wennberg, P. O., Wofsy, S. C., Stephens, R. S., Fischer, M. K.R., Uchino, O., Abshire, J., Bernath, P., Biraud, S., Blavier, J., Boone, C., Bowman, K. P., Browell, E. V., Campos, T., Connor, B., Daube, B. C., Deutscher, N. M., Diao, M., Elkins, J. W., Gerbig, C., Gottlieb, E., Griffith, D. W., Hurst, D. F., Jimenez, R., Keppel-Aleks, G., Kort, E. A., Macatangay, R., Machida, T., Matsueda, H., Moore, F., Morino, I., Park, S., Robinson, J., Roehl, C. M., Sawa, Y., Sherlock, V., Sweeney, C., Tanaka, T., and Zondlo, M. A.: Calibration of the Total Carbon Column Observing Network using aircraft profile data. Atmospheric Measurement Techniques, 3 (5), 1351-1362, 2010

Wunch, D., Toon, G. C., Blavier, J.-F. L., Washenfelder, R. A., Notholt, J., Connor, B. J., Griffith, D. W. T., Sherlock, V., and Wennberg, P. O.: The Total Carbon Column Observing Network,

Philosophical Transactions of the Royal Society A, 369, 2087-2112,  
doi:10.1098/rsta.2010.0240, 2011.

Xu, X. F., Tian, H. Q., Zhang, C., Liu, M. L., Ren, W., Chen, G. S., Lu, C. Q., and Bruhwiler, L.: Attribution of spatial and temporal variations in terrestrial methane flux over North America, Biogeosciences, 7, 3637-3655, doi:10.5194/bg-7-3637-2010, 2010.

Zhang, Z., Zimmermann, N. E., Kaplan, J. O., and Poulter, B.: Modeling spatiotemporal dynamics of global wetlands: comprehensive evaluation of a new sub-grid TOPMODEL parameterization and uncertainties, Biogeosciences, 13, 1387-1408, <https://doi.org/10.5194/bg-13-1387-2016>, 2016.

Zhao, Y., Saunois, M., Bousquet, P., Lin, X., Berchet, A., Hegglin, M. I., Canadell, J. G., Jackson, R. B., Hauglustaine, D. A., Szopa, S., Stavert, A. R., Abraham, N. L., Archibald, A. T., Bekki, S., Deushi, M., Jöckel, P., Josse, B., Kinnison, D., Kirner, O., Marécal, V., O'Connor, F. M., Plummer, D. A., Revell, L. E., Rozanov, E., Stenke, A., Strode, S., Tilmes, S., Dlugokencky, E. J., and Zheng, B.: Inter-model comparison of global hydroxyl radical (OH) distributions and their impact on atmospheric methane over the 2000–2016 period, Atmos. Chem. Phys., 19, 13701–13723, <https://doi.org/10.5194/acp-19-13701-2019>, 2019.